JTTEE5 14:125-133
DOI: 10.1361/10599630522738
1059-9630/$19.00 © ASM International

A Systematic Approach to Material Eligibility for the Cold-Spray Process

J. Vlcek, L. Gimeno, H. Huber, and E. Lugscheider

(Submitted August 28, 2003; in revised form December 22, 2003)

This article represents an effort to systematize an understanding of the cold-spray process and the suitability of materials for such a process. The evaluation is based on a brief analysis of the powder particle impact and literature research concerning shock-compression phenomena in matter and related physical effects, such as impact heating and dynamic yielding. The finite-element modeling (FEM) allows the estimation of the maximum impact pressures, the deformation rates, and the deformation kinetics during impact. The calculations can be verified experimentally and are supported by the published data. From a brief analysis of the equations of state applied to shock compression, key material parameters are derived and investigated. A parameterization of physical properties and correlation with the crystal types endeavors to provide a qualitative ranking of material suitability.

Keywords cold spray, dynamic yielding, high strain rate deformation, impact heating, material properties

1. Introduction

Kinetic compaction encountered in the cold-spray process is characterized by the solid-state, high-velocity impact of powder particles onto the substrate, leading to high-pressure loading of the powder feedstock and substrate. It is generally accepted that the material sprayed must feature a minimum ductility to allow for clamping, shearing of the particle surfaces, and cold welding. Melting could be detected for some materials such as Ti-6A1-4V alloy (Ref 1), but for other metallic materials high deformation and shear phenomenon were observed and documented. So far, no general rule could be applied to determine whether a material can be processed by means of the cold-spray process, although the concept of evaluating materials by the critical velocity necessary for their deposition is well accepted to explain bonding and jetting phenomena (Ref 2-5).

According to the shock theory of impact dynamics, a pressure shock during impact and the resulting plastic shock wave will lead to substantial deformation of the particle during impact. By means of the equations of state, the maximum impact pressures can be estimated, showing that for a velocity regimen well above 1000 m/s, peak shock pressures of 40 to 50 GPa are possible for iron- and copper-base materials.

Due to the nature of the impact kinetics, the pressure rise and drop is rapid, as finite-element modeling (FEM) simulations confirm. Data published for the dynamic compaction of powder show that the pressure rise time is a key variable for good bonding between powder particles (Ref 6, 7). Depending on the plastic behavior and specific dynamic yield strength of the material sprayed, elastic load relief will take place below a critical pressure, possibly leading to debonding if a good cold weld is not developed.

The deformation kinetics are determined by the material properties, mainly the crystal and grain structure, as well as by the type of bonding within the material. The Grüneisen parameter is key in the calculation of shock pressure and dynamic yielding and combines the mechanical as well as thermodynamic properties of a material. This article discusses the properties of metals and ceramics to give a rating for their cold-spray suitability. The results can be confirmed empirically through the experiments performed and data published so far, demonstrating that feedstock properties are the key variables in the cold-spray process.

This article does not discuss the interaction between the particle and the substrate in detail. The analysis is concentrated on the properties of the material sprayed, but the influence of the particle-substrate interaction has to be acknowledged for the initial phase of deposition (Ref 3, 8). Nevertheless, coating buildup in the cold-spray process will be governed mainly by the material sprayed, because it is deposited layer by layer. It also has to be remarked that the results are presented under the assumption of continuum mechanics even though anisotropic effects might need to be considered as investigations (Ref 3) indicate.

2. High-Velocity Impact

The principle underlying the cold-spray process is to accelerate powder particles in a supersonic gas jet onto a substrate to generate a coating solely through the shear and cold-welding processes that occur between the particles or particles and the substrate upon impact with typical velocities above 700 m/s. Since the first publications by McCune et al. (Ref 2) and Alkimov et al. (Ref 9), the process technology has been described often and is not explained further here. The high-velocity

The original version of this article was published as part of the ASM Proceedings, *Thermal Spray 2003: Advancing the Science and Applying the Technology*, International Thermal Spray Conference (Orlando, FL), May 5-8, 2003, Basil R. Marple and Christian Moreau, Eds., ASM International, 2003.

J. Vlcek, L. Gimeno, and **H. Huber,** EADS GmbH, Postfach 80 04 36, 81663 Munich, Germany; and **E. Lugscheider,** Material Science Institute, University of Technology, Aachen, Germany. Contact e-mail: Johannes.vlcek@eads.net.

impact of powder particles in the solid state was simulated numerous times to examine the marginal conditions of the cold-spray process more closely (Ref 3, 5, 10, 11). Jetting phenomena could be detected for numerous particles and different materials, although melting could only be documented in rare cases, such as that for Ti-6Al-4V alloy at the bonding interface of particles at the pressed-out material jet (Ref 1). Jetting can be related to the shock propagation in the particle (Ref 12) and, consequently, to the velocity of the particle at impact (Ref 5).

The deformation kinetics and the dependence of the impact pressure in terms of time in the cold-spray process were simulated by means of the explicitly dynamic FEM Code LS-DYNA3D (LSTC = Livermore Software Technology Corp., Livermore, CA) for 316L material. Here, for both the particle and substrate material, a strain-rate-dependent and temperature-dependent material model for the 316L alloy modified according to Zerilli-Amstrong (LS-DYNA3D, Standard Material Model 65) was used (Ref 13). In the simulation, due to the brevity of the deformation process ($<10^{-4}$ ms) adiabatic deformation was assumed, and it was presumed that 90% of the plastic work was converted into a temperature increase. The modeling is not a coupled thermal/mechanical analysis.

In the simulation, the marginal conditions were reduced to the two-dimensional model of a hemisphere, which is permissible in view of the rotationally symmetric deformation of the spherical particle. The diameter d_P of the particle is 20 µm. The substrate material is modeled as a cylinder having a diameter of $3 \times d_P$ and a height of $5 \times d_P$. The network was generated correspondingly and was refined in areas with a high deformation.

The simulation yields the equivalent total strain e_V, and the stresses occurring in x, y, and z direction. The analysis of the equivalent total strain in the particle and in the substrate as the particle velocity increases has already been described elsewhere (Ref 1, 11). The results show that, as the particle velocity increases, the deformation of the particle increases and the substrate is penetrated to a greater extent.

The contact pressure occurring in the impact direction (y-direction) as a result of the impact depends directly on the particle velocity. The pressure is greatest in the first phase of the impact. Shortly after the first contact at time $t_S = 4.9 \times 10^{-6}$ ms, a maximum pressure of >13 GPa can be calculated for an impact velocity v_P = 700 m/s for the 316L alloy particles on a 316L substrate. The peak pressure acts for $<1.0 \times 10^{-5}$ ms, followed by a significant drop to below 3 GPa. The progression versus time can be explained very simply through the increase of the effective contact area A_P between particle and substrate, and the associated decrease of the quotient $\sigma_y = F/A_P$, where F is the impact force of the particle acting on the contact area. In the boundary case of the first contact, the area is only a point (σ_y versus ∞), whereby, as particle deformation increases, the contact area A_P increases and therefore the stress σ_y drops. Corresponding $\sigma_y - t_S$ progressions are shown in Fig. 1(a) as a function of the particle velocity v_P. A peak stress σ_y of almost 25 GPa is reached upon impact of a particle at 1200 m/s. When v_P = 1200 m/s, at the simulation time $t_S = 2.0 \times 10^{-5}$ ms, a positive stress σ_y is reached, which might indicate a load-relief pressure wave in the material. Figure 1(b) depicts the distribution of the stress σ_y, which corresponds to the pressure in the y-direction, of a particle impinging at 700 m/s at time $t_s = 2.0 \times 10^{-5}$ ms. A maximum pressure of 2.69 GPa occurs in the area of the contact zone below the particle center.

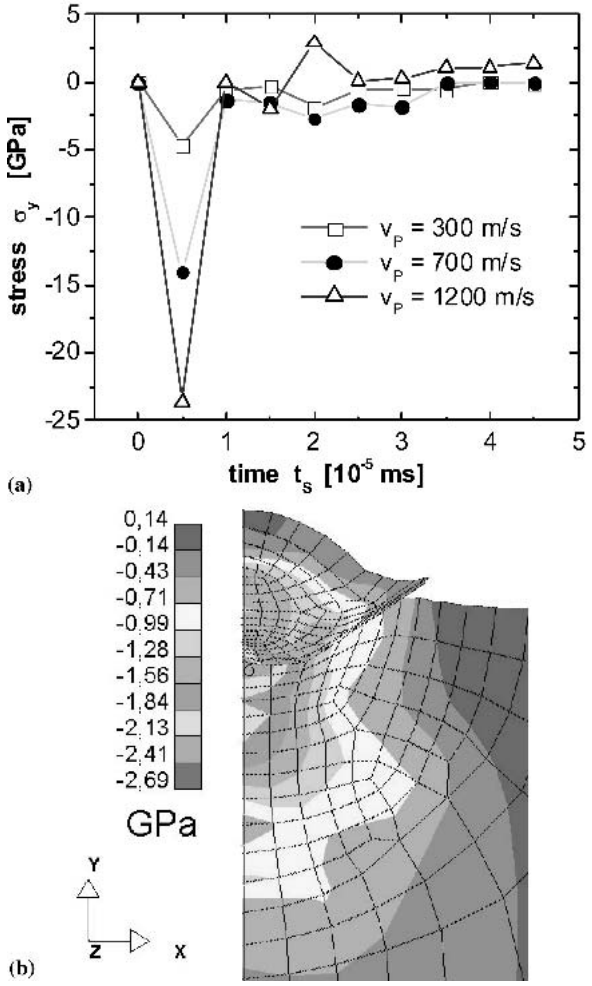

Fig. 1 (a) Calculated stress progression σ_y versus the simulation time t_S at the point of particle-substrate (316L material) contact below the particle center. (b) Stress distribution σ_y in a 316L particle impacting a 316L substrate: $d_P = 20$ µm and $v_P = 700$ m/s, at time $t_S = 2.0 \times 10^{-5}$ ms

In scanning electron microscopy investigations, the morphology of the particles and the penetration of the substrate that was calculated in the FEM simulations can be verified. Here, Fig. 2 illustrates the analysis of a 316L particle on a carbon steel substrate. A comparison between Fig. 1(b) and 2 demonstrates that the penetration of the substrate is not as pronounced as the FEM simulations show. The formation of the material jet at the particle/substrate interface can be seen clearly (arrow). Further investigations show that the material properties of the particle and the substrate determine the penetration of the substrate, as well as the deformation of the powder particle and the substrate (Ref 8). Consequently, 316L particles are hardly deformed upon impact on aluminum. In contrast, copper particles can hardly cause craters in steel substrates. Accordingly, the specific properties of particle and substrate are decisive, as far as bonding and coating formation are concerned.

3. Impact Heating

The high-speed impact during the cold-spray process corresponds to a shock load on the particle material and the adjacent

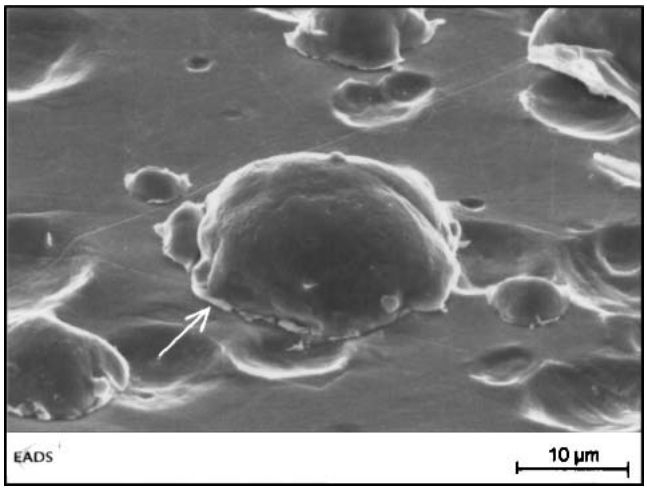

Fig. 2 A 316L particle upon impact on a polished steel substrate

substrate areas. A fundamental description of the behavior of metals subjected to compression due to shock waves is given by the curve of the equations of state, also called the Hugoniot curve (Ref 14-16). Most frequently, the interaction of the shock-wave parameters is represented in the pressure-specific volume (*p-V*) relationship, as shown in Fig. 3. The Hugoniot curve indicates the final states reached during exposure to a shock wave, but not the intermediate states that are passed through, and depends on the material properties. The connecting line between the starting point and end point is termed the Raleigh line and characterizes the shock-wave velocity. The area under the Raleigh line reproduces the increase of the internal energy, which increases as the temperature rises up to the shock temperature. The load relief after the shock wave has passed through occurs along the load-relief isentropes, whereby the irreversibly remaining shares of the energy cause the material to warm up. The higher temperature leads to a higher volume of the material traversed by the shock wave, which is larger than the initial volume. The volume increase is illustrated in Fig. 3, because the volume V_E traversed by the shock wave is greater than the initial volume V_0.

In general, the Hugoniot curve and the relief adiabatics deviate only slightly from one another, so that, in contrast to the shock temperature, only slight residual temperatures occur (Ref 14). For metals, Hugoniot curves exhibit continuous compression with increasing shock-wave pressure. Iron exhibits unsteadiness at 13 GPa, at which transformation from α-iron (Fe) to γ-iron occurs, induced by the pressure. The shock-wave temperatures in comparison to the residual temperatures are shown in Fig. 4. Aluminum (Al) exhibits, at 500 °C and approximately 28 GPa, the highest shock temperatures, and copper (Cu), at <150 °C, the lowest ones. At this pressure, the residual temperatures rise for Cu, Fe, and Al at less than ~150 °C.

The globally reached residual temperatures do not permit the materials to melt. In the highly deformed bonding interface, in which material may be pressed out, melting is, however, generally conceivable due to the pronounced shear processes and the high-impact pressures. The analyses of sprayed Ti-6Al-4V specimens show that local melting occurs on the material jet formed in the bonding interface (Ref 1).

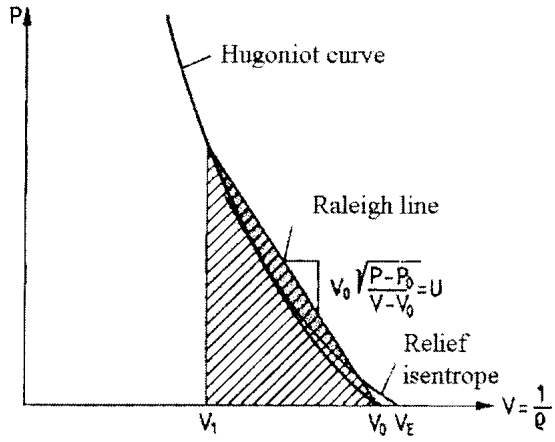

Fig. 3 Schematic Hugoniot curve (Ref 14)

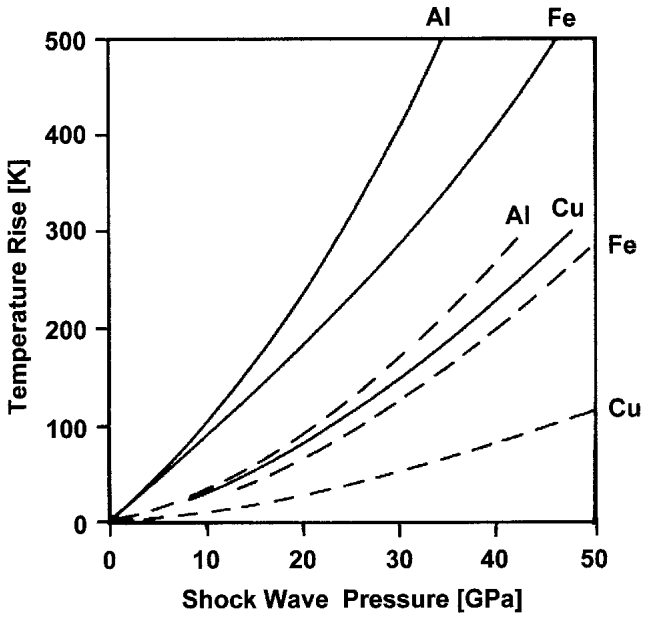

Fig. 4 Comparison between shock temperature and residual temperature (dashed lines) as a function of the shock-wave pressure (Ref 17-19)

4. Equations of State

In mathematical terms, the behavior of shock waves in the material is described by the laws of the conservation of mass, the conservation of impulse, and the conservation of energy versus the shock front. For the general case of a body traversed by a shock wave and having the state t_0 before the shock-wave front and the state t_1 just behind the shock, the general balance equations are given in all standard works on the shock-wave propagation in solid bodies (e.g., Ref 14-16). The Hugoniot curve can be calculated from these equations.

Besides the above-chosen depiction of the Hugoniot curve in the *p-V* relationship, a simple representation of mass velocity u (u_1) versus shock-wave velocity U is customary. For most metals, a linear relationship applies at mean pressure levels between mass velocity and shock-wave velocity, so that the *u-U* curve can be described by the following straight line (Ref 15):

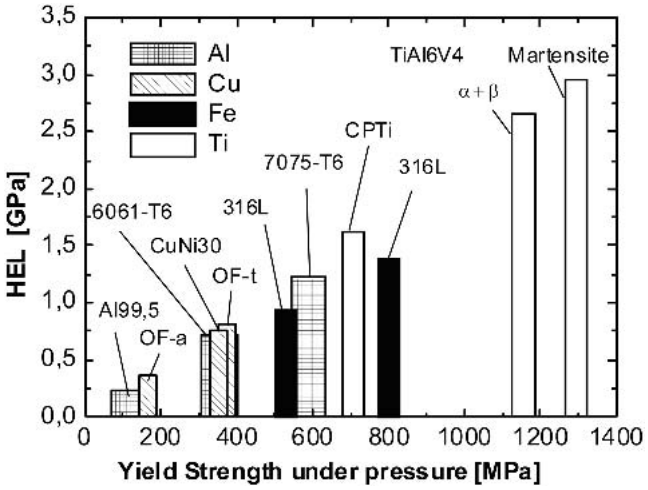

Fig. 5 Calculation of the HEL according to Eq 3 (Ref 15, 20-23)

$$U = C_0 + S \cdot u \text{ with } C_0 = \sqrt{\frac{K}{\rho_0}} \quad \text{(Eq 1)}$$

where S depends on the material properties, which are combined in the Grüneisen parameter Γ (Ref 15):

$$S = \frac{1}{2} \cdot (1 + \Gamma) \text{ with } \Gamma = \frac{3 \cdot \alpha K}{\rho_0 \cdot c_v} \quad \text{(Eq 2)}$$

The Grüneisen parameter Γ describes the relationship between internal energy and pressure at a constant volume. The linear coefficient of expansion α, the thermal capacity c_V, the density ρ_0, and the modulus of compression K are included. The flow of the material occurs at the flow limit Y_0, defined by the criterion established by Mises and Tresca $Y_0 = \sigma_x - \sigma_y$ at:

$$\sigma_{HEL} = \left(\frac{K}{2G} + \frac{2}{3}\right) \cdot Y_0 \quad \text{(Eq 3)}$$

and is termed the Hugoniot elastic limit (HEL). At this limiting stress, the elasticity of the material is exceeded, and a transition occurs from the elastic to the plastic shock wave, with plastic deformation of the material (Ref 14, 15). For mean shock-wave pressures of up to ~10 GPa, K and G are pressure-independent constants (Ref 15).

5. Dynamic Yielding

Depending on the material characteristics, the uniaxial description of the dynamic flow limit σ_{HEL} Eq 3 renders it possible to estimate the limiting stress with respect to the plastic deformation of the shock-loaded material in the first order. Zukas (Ref 15) provided the simple estimate $Y_0 = 3.92 \times$ HB in MPa, where HB is the Brinell hardness of the material. Figure 5 illustrates calculations concerning the HEL for various materials. The elastic yield strength is illustrated for specific materials exposed to pressure as well as the corresponding dynamic flow limit. Values of <0.5 GPa are calculated for aluminum and copper (very low flow limits), as well as values of almost 3 GPa for Ti-6Al-4V in its rapidly solidifying, martensitic form, which is typical of an atomized powder material. A high dynamic flow limit indicates substantial deformation forces and poor compressibility. For a 316L alloy, depending on the strain hardening, a value between 0.9 and 1.5 GPa is calculated for σ_{HEL}. The values for annealed copper and tempered copper vary somewhat between 0.4 and 0.8 GPa, respectively. The material properties used for the calculations are taken from Ref 15, 20-24.

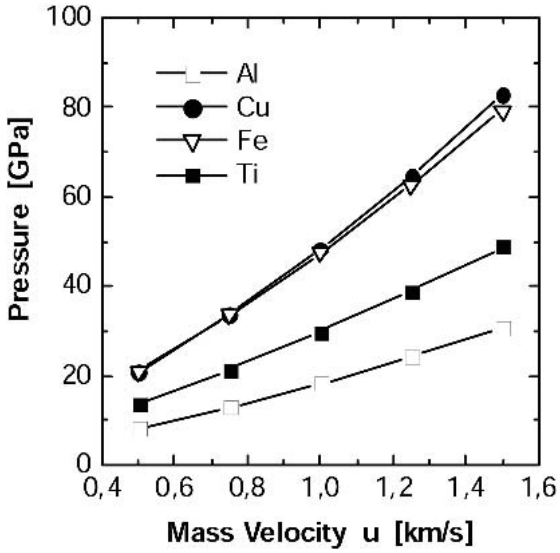

Fig. 6 Calculation of the shock pressure in the material as a function of the mass velocity u and the Grüneisen parameter Γ, at the moment of impact: $u = v_P$ applies (Ref 15, 20, 24)

6. Impact Pressures on Materials

The impact of the powder particles onto a substrate can be subdivided into two phases:

- Pressure buildup and the elastic deformation of the particles up to the dynamic flow limit upon exposure to pressure
- Plastic deformation with significant deformation of the material structure and warming due to deformation

The simulation shows that the contact pressure on impact of the particles rises suddenly and that the elastic phase of the impact is virtually negligible, assuming that there are sufficiently high impact velocities that lead to the exceeding of the flow limit. Applying Eq 1 and assuming the conservation of the impulse, the pressure upon impact can be estimated easily. Figure 6 depicts the pressure as a function of the mass velocity u in the material in a P-u diagram. For the moment of impact, $u = v_P$ can be set. For particle velocities v_P = 500 m/s, impact pressures of up to 20 GPa occur. For the materials Al, Cu, Fe, and Ti, very different pressures are reached. The differences in pressure are determined by the material properties, combined in the Grüneisen parameter Γ. The elastic and physical material characteristics are included in Eq 2. The main parameter of influence is the modulus of compression, whereby large values lead to high pressure on impact. The estimate is simplified and is relative to

the ambient temperature, but good compliance with Hugoniot data is to be found in the literature (Ref 16, 25).

A comparison with Fig. 5 shows that on impact the dynamic flow limit for the materials studied is certainly exceeded and that pronounced plastic deformation takes place. As far as the impact kinetics are concerned, the length of time for which the plastic pressure wave can act with a pressure above the dynamic flow limit is decisive. The calculations in the FEM model (Fig. 1), show that at v_P = 700 m/s, pressures of ~2.5 GPa act during impact for about 3×10^{-5} ms in the bonding interface (i.e., 20 μm for a 316L particle on a 316L substrate). The impact kinetics are thereupon ended. The pressure lies clearly above the dynamic flow limit. According to the calculated pressure distribution, after the first contact far lower pressures act but are still larger than the dynamic flow limit. The propagation of the shock wave can explain the heterogeneous deformation of the particles observed on sprayed samples. A spherical shock wave starting from the first point of contact and rapidly losing energy due to surface increase can serve as a simple model. In the two-dimensional plot of the particle (Fig. 1b), the close-to-circle-shaped regions of constant pressure are visible. The FEM calculations were not evaluated further to define a line of deformation in the particles or to evaluate possible relief adiabatics.

7. Classification of Material Behavior

Particle impact is, in the first instance, a plastic deformation process. Mechanical material models describe the behavior of a material during the deformation process via the relationship between true elongation and true stress (i.e., the yield criterion value). Values published in the literature show clearly that the yield criterion values of Al-, Cu-, and Fe-base materials differ greatly (e.g., Al-to-steel ratio = 1 to 5 at a true elongation of 0.4) (Ref 26, 27). The particle materials as well as the substrate materials, Al, Cu, steel, and hardened steel, experience deformations as a function of their yield criterion value.

The deformation strain rate on particle impact is extremely high ($d\varepsilon/dt > 1 \times 10^5$ s^{-1}), which is why additional strain-hardening effects due to the accumulation of dislocations, interactions of the atoms among one another, and, if appropriate, a temperature-induced decrease in the yield criterion value should be taken into consideration. Consequently, for the strain-hardening alloy 316L it is difficult to generate dense coatings. The Ti-6Al-4V alloy exhibits a decrease in strain hardening at temperatures below the β-transition and can only be cold-worked with difficulty (Ref 21, 26), which explains the high porosity and cracks in the corresponding coatings. In the cold-spray process, the response of the materials to high-velocity deformation and the associated strain rates of $>1 \times 10^5$ s^{-1} is decisive.

Mechanical material models do not portray what actually happens during deformation inside the metals. The deformation process is determined by the mobility of the dislocations and their interactions in the deformation process (Ref 28). Consequently, in particular the crystal structure and the type of bonding as well as further parameters, such as structure, grain size, and foreign atoms or phases, determine the resistance to deformation. Comparing the deformation properties of different metals shows clearly that metals of one crystal structure and type of bonding feature similar deformation mechanisms (Ref 29). Hence, polycrystalline solids can be classified into isomechanical groups (i.e., groups that combine similar mechanical properties). They form subgroups within a crystal structure. The most important isomechanical groups of metals are (Ref 29):

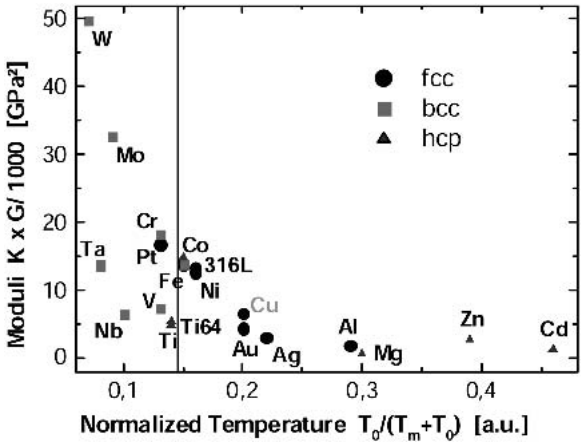

Fig. 7 Parameterized representation of the plastic properties of various materials (the product of the shear modulus and the modulus of compression) as a function of the normalized temperature $T_0/(T_0 + T_m)$ with T_0 = 273 K and T_m is the melting temperature of the material. Characteristics are for T = 293 K (Ref 20).

- Al, Cu, Ag, Au, Pt, Ni, and γFe oriented face-centered cubic (fcc)
- W, Ta, Mo, Nb, V, Cr, αFe, and βTi oriented body-centered cubic (bcc) (also transitional states)
- Cd, Zn, Co, Mg, and Ti close-packed hexagonal (cph)

The fcc metal structure features the greatest packing density (PD = 12), coordination number (KZ = 12), and a large number of sliding planes, which explains the good deformability (Ref 28). The structure with cph features the same PD, but, due to the spatial arrangement in a tight stacking sequence, the number of sliding planes is greatly reduced, resulting in poorer deformability. The bcc metal structure has a significantly lower PD (0.68) and KZ (8), which is why it should be assigned the lowest deformability of the three structures. Groups of tetragonal or trigonal crystal systems include oxides, which, due to their low plasticity, are not suitable for the cold-spray process.

A correlation between deformation properties and bonding type for the three isomechanical groups is supplied by plotting the product of the shear modulus and the modulus of compression as a function of the normalized temperature $T_0/(T_0 + T_m)$ with T_0 = 273 K and T_m is the melting temperature of the material (Fig. 7). The product of shear modulus and modulus of compression takes into consideration two important material parameters and clarifies the distribution of the data points.

The representation permits a rough classification of suitability for the cold-spray process. Copper, which can be regarded as being an almost ideal material, features a low resistance to deformation at a melting temperature of <1100 °C. Materials with a low melting temperature can be compacted easily. Verified

empirically, the plotted line corresponds to a T_m of ~1600 °C, at which temperature difficulties must be expected with regard to compacting. At the correspondingly high particle velocities, coatings can be made that, as the case may be, feature increased porosity (e.g., with Ti-6Al-4V alloy). For materials with a higher resistance to deformation and higher melting temperature, for the most part no coatings can be built up or extreme parameters must be selected. Figure 7 illustrates the specific distribution of the isomechanical groups, whereby it is generally more difficult to process the bcc metals in the cold-spray process because at deformation under high strain rates, screw dislocation mobility is strongly hindered by Peierls stress.

8. Discussion

Typical of the high-velocity impact of the powder particles in the cold-spray process is the high deformation velocity in the material, which, as a rule, leads to high deformation and temperature effects. The cause of deformation and strain hardening of the material is a plastic shock wave passing through the particle, which acts as a result of the high impact pressure.

The extremely rapid rise in pressure upon particle impact is an important characteristic of the process, which probably serves to achieve the bonding of the powder particles. Raybould (Ref 6) and Lemcke and Raybould (Ref 30) showed in calculations and experiments that the time needed for the pressure to rise (i.e., shock rise time (SRT)) and an adequate duration of the plastic pressure wave represent the prerequisites for melting. Here, the SRT must be shorter than the time in which the shock-induced heat is dissipated. The calculations show that the peak pressure is built up in $<10^{-8}$ s. For Ti-based materials, evidently during this time only, slight heat dissipation occurs, so that melting may take place in the bonding interface, as is indicated in the investigations by Vlcek et al. (Ref 1).

The FEM calculations show that peak pressures of up to 25 GPa can be expected for a 316L alloy at impact velocities of 1200 m/s (e.g., a 20 μm particle on 316L substrate). Due to the deformation kinetics with a continuously increasing contact area between particle and substrate, the maximum pressure decreases very rapidly. The FEM calculations and analyses on thermally sprayed materials show that the impinging powder particles are deformed only heterogeneously (i.e., on the substrate side). The deformation of the entire particle is not possible, as the plastic shock wave weakens rapidly as the surface of the shock front increases. When the HEL, as the material-specific limit pressure (limiting stress), falls short, the transformation into an elastic shock wave takes place.

Simple estimates of the HEL (Fig. 5) and the comparison with the pressures acting upon impact (Fig. 6) show that the limiting stress is certainly exceeded upon impact. However, the deformation kinetics are the cause of the HEL being underrun, depending on the material, after the first contact, as the case may be. For Ti-base materials, the limiting stress is high, which explains the poor processibility in the cold-spray process. Figure 6 clarifies that far lower impact pressures are reached for Ti than, for example, for Cu, which can be regarded as being a further indication of poorer suitability. Cu-base materials feature a very low limiting stress, and high impact pressures are reached, which is why plastic deformation up to the end of the deformation kinetics can be assumed. Dense aluminum material can be sprayed easily in the cold-spray process (Ref 2, 9, 10), which can easily be understood by analyzing the high shock temperatures, the low dynamic flow limit, and the low yield criterion value, which is greatly influenced by a temperature increase to above 150 °C (Ref 26, 27). In contrast, for specific Al alloys, well-bonded and dense coatings can be realized only with difficulty, which correlates with the higher HEL and the generally low impact pressures of Al-base materials, as shown in Fig. 5 and 6.

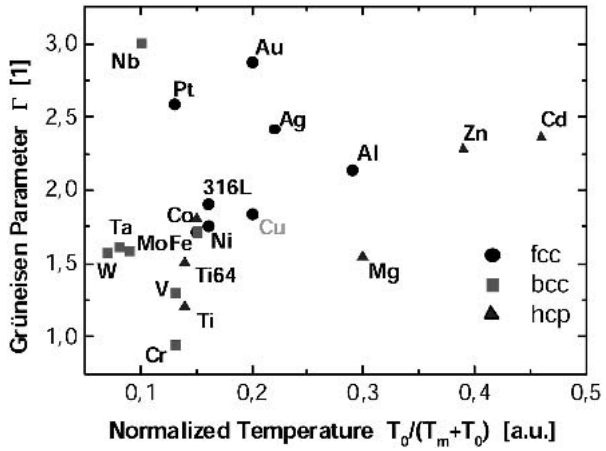

Fig. 8 Parameterized representation of the relationship between internal energy and pressure at a constant volume versus the Grüneisen parameter Γ as a function of the normalized temperature $T_0/(T_0 + T_m)$ with T_0 = 273 K and T_m is the melting temperature of the material. Characteristics are for T = 293 K (Ref 20)

Classifying the metals by isomechanical groups, defined according to the classification of Frost and Ashby (Ref 29), reproduces the general suitability for the cold-spray process. Here, the generally known characteristics of the deformability of the materials are correlated with their crystal structure. Body-centered cubic materials usually prove to be difficult in the cold-spray process (i.e., processing with helium is the only alternative to obtain pore-free coatings). At moderate strain rates, some bcc metals may deform in a manner that is similar to that of fcc metals, but at the strain rates that are typical for the cold-spray process the necessity to activate screw dislocation movement (which needs more energy than edge dislocations in an fcc matrix) makes this type of metal significantly more difficult to deform plastically. Low-melting-point cph metals have been found to be easy to process. This proves that, besides the mechanical characteristics, other features such as the bonding energy must be taken into consideration.

The parameterization of the materials illustrated in Fig. 7 relates to the data concerning customary deformation rates in the range of 1 to 10 s^{-1} and ambient temperature. This is the reason for the main inaccuracy and is the reason why the results can only be regarded as a first estimate. A parameterization versus the Grüneisen parameter Γ (compare with Eq 2) provides a comparable classification of the materials, as is shown in Fig. 8. The cause is the great influence of the modulus of compression K on the value of the Grüneisen parameter. Attempts to relate the suitability for the cold-spray process to values such as those for

Peierls stress appear to be appropriate from the materials point of view. The Peierls stress together with the stacking fault energy are a measure for the energy necessary to move dislocations or enable twinning in a lattice, both of which are important characteristics of deformation processes. Data for the corresponding values at ambient temperature and above have not been found to date. According to Frost and Ashby (Ref 29), the material characteristic of phonon drag is decisive for extremely high deformation rates in the case of the deformation assumed in a first approximation as being Newtonian-viscous. No data have been found in the literature as yet.

Over and above this, in the cold-spray process further marginal conditions must be taken into account. Due to its low strength, magnesium offers very good prerequisites for the process (see Fig. 7, 8) but necessitates, due to its low density and the resultant low impinging impulse, high particle velocities to ensure adequate impact pressures. However, due to the low melting temperature, the process window is limited to low gas temperatures, which gives rise to a fundamental problem with regard to processibility. Today, processing is often limited for many materials by nozzle fouling, but this might be solved in the future by nozzle optimization. Consequently, besides judging the suitability of a material on the basis of its characteristics, the marginal process conditions must therefore be taken into consideration, in particular the limits of the particle condition parameters v_P and T_P. Further, good coating qualities have been reported for tantalum and niobium, so that the limit, now associated empirically with the Ti-6Al-4V alloy, does not provide an adequate differentiation of suitability (Ref 31).

In Fig. 9, an attempt to relate the discussed material properties under high-velocity impact to process conditions has been made to give a first explanation for why certain materials can be cold sprayed and some cannot. The "process grid" relates the dynamic yield strength (see Fig. 5) and the impact pressure (Fig. 6) with an important process condition, the kinetic energy of the particle, and with the material type of bonding, represented by its melting temperature. All data are normalized to the values calculated for tungsten (W) as a reference. Substrate properties are not considered. The kinetic energy of the particle is a measure of the overall energy available during the particle impact and is dependent on the particle velocity, diameter, and density. For the calculation presented, 20 μm particles with a velocity of 700 m/s were assumed.

The high dynamic yield strength of Ti, the lower impact pressures than Cu, and a reduced kinetic energy are obvious, and indicate the difficulties when cold spraying Ti, as discussed before. Tantalum (Ta) shows higher dynamic yield strength than Cu, but impact pressures are about 50% higher. Additionally, due to their high density, Ta particles with comparable size and velocity yield higher kinetic energy than Cu particles. For Mg, properties similar to those for Al can be calculated, but a lower kinetic energy, a consequently lower overall energy available for deformation, and considerably lower impact pressures have to be acknowledged. The "process grid" shows a correlation between relevant particle parameters, which characterize the material behavior during the particle impact. Distinct differences for specific materials can be shown, which might give some indication for why the materials discussed above, Ta and Mg can be easy or difficult to process, respectively. The inaccuracies discussed before certainly apply, but a multiple comparison of process variables can help greatly to estimate material suitability for the cold-spray process.

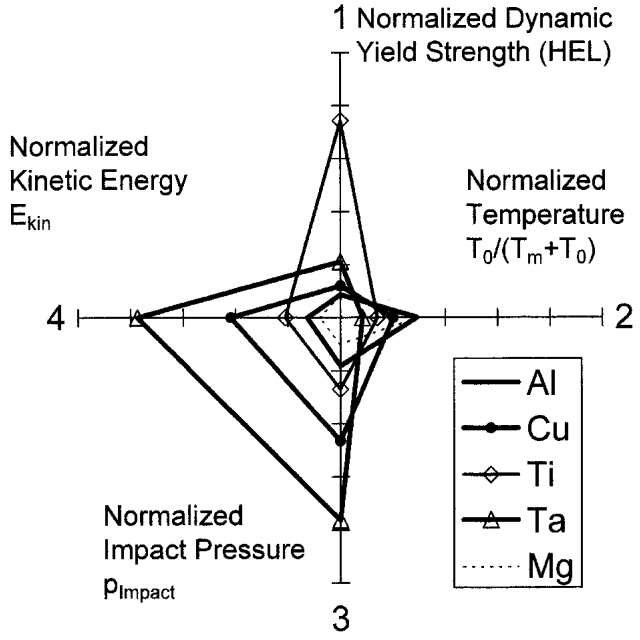

Fig. 9 Parameterization using a normalized process grid that combines the discussed characteristics of high-velocity impact, dynamic yield strength, impact pressure, the material bond through the melting temperature of the material sprayed, and the kinetic energy available during impact calculated for a 20 μm particle at a particle velocity of 700 m/s. The data are normalized against a calculation for W material properties, which yields the highest values for all parameters. All material data are given according to the sources cited in Fig. 5 and 6. Substrate properties have not been considered for this evaluation.

Experiments on nanostructured oxide ceramics (Ref 32) show that these materials too can be processed with certain restrictions. The metallographic cross section of a ZrO_2 coating produced with the cold-spray process is depicted in Fig. 10. However, it looks like its deposition is limited to monolayers, but nevertheless it was possible to generate very thin and dense coatings. There is as yet no explanation as to the bonding mechanism between particles of the oxide ceramics.

9. Summary and Conclusion

In connection with the cold-spray process, this article has examined the typical characteristics of the deformation kinetics, the maximum pressures that occur, and the material-specific parameters that determine the high-velocity impact. It becomes clear in the simple analyses that the process leads, in the case of most materials, to high plastic deformation as the dynamic yield strength is exceeded. Elastic deformation can probably be neglected in a first approximation.

The summarizing evaluation of the results shows that judging the suitability of materials for the cold-spray process must be effected on the basis of the deformation properties. The mobility of the dislocations in the crystal lattice drops in a graded classification of the crystal structures, namely, fcc, cph with the great-

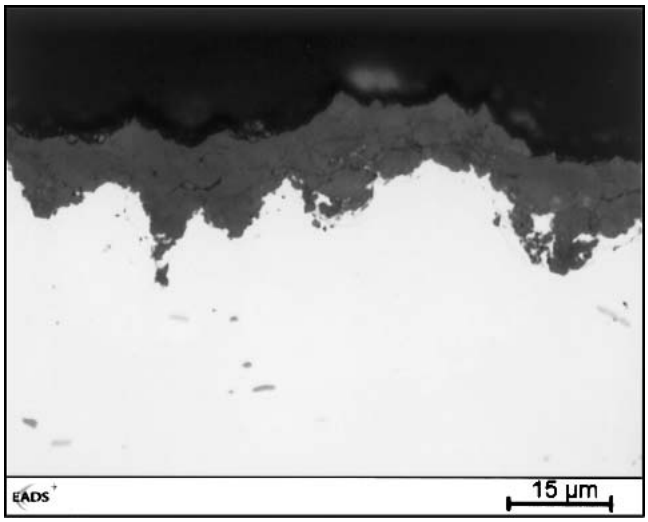

Fig. 10 A ZrO_2 coating produced with the cold-spray process using helium as the process gas at a temperature of 773 K. The substrate is Al. The feedstock material, produced by a sol gel technique and stabilized with ceria, had a nanoscale structure.

est density, and bcc. The deformability in the cold-spray process, and hence the suitability of the materials, drops correspondingly. In addition, the bonding type of the molecules, characterized in a simplified manner by the melting temperature, can be used as an evaluation criterion. At approximately 1600 °C, a significantly more difficult compactability is to be defined in the cold-spray process on the basis of the experiments and the data published in the literature.

Classifying the materials by means of the parameterizations described here can only be regarded as being a rough framework, but it shows clearly that materials that are very suitable for the cold-spray process have a low melting point and low mechanical strength. Zn, Al, and Cu are ideal materials, as they have a low yield strength and exhibit clear softening at elevated temperatures. No gas prewarming or only low process temperatures are required to produce dense coatings from these materials. In contrast, for the majority of the Fe- and Ni-base materials, the generally low process temperatures have a disadvantageous effect. The process supplies, in an energetic context, insufficient overall energy for these materials to produce dense coatings and high application rates. However, niche applications do indeed evolve for the cold-spray process on the basis of the low process temperatures, where the locally restricted buildup of a coating and the low oxidation of the substrate and the powder material used for spraying are required.

The systematic approach described in this article permits judging, on the basis of the characteristics of the particle that can be determined in a simple manner (e.g., material hardness, melting temperature, and basic physical data, as well as particle velocity or density), the suitability of a material for the cold-spray process.

The qualitative approach to compare the ability of materials to bond in cold spraying by a simple formula (Ref 5) is also based on similar input data such as the density and melting temperature of the material, the tensile strength, and the particle temperature. The ranking of the materials discussed corresponds to the analysis given here. Therefore, evidence is given that the critical velocity related to specific materials and the phenomenon of jetting are closely linked to shock-compaction phenomena in matter. Further studies should look more closely at the interaction of shock-wave propagation in the particle and substrate material because this interaction, especially during the deposition of the first layer, will determine whether bonding, debonding, or jetting occurs.

References

1. J. Vlcek, H. Huber, H. Voggenreiter, and E. Lugscheider, "Melting Upon Particle Impact in the Cold Spray Process," presented at Materials Week 2002, International Congress on Advanced Materials, Their Processes and Applications, *Deutsche Gesellschaff fur Materialkunde* (DGM) (Munich, Germany), Sept 2002
2. R.C. McCune, A.N. Papyrin, J.N. Hall, W.L. Riggs, and P.H. Zalchowski, An Exploration of the Cold Gas-Dynamic Spray Method for Several Material Systems, *Advances in Thermal Spray Science & Technology,* Sept 11-15, 1995 (Houston, TX), C.C. Berndt and S. Sampath, Ed., ASM International, 1995, p 1-5
3. R.C. Dykhuizen, M.F. Smith, D.L. Gilmore, and R.A. Neiser, Impact of High Velocity Cold Spray Particles, *J. Thermal Spray Technol.,* Vol 8 (No. 4), 1999, p 559-564
4. T. Stoltenhoff, H. Kreye, H.J. Richter, and H. Assadi, Optimization of the Cold Spray Process, *Thermal Spray 2001: New Surfaces for A Millennium,* May 28-30, 2001 (Singapore), C.C. Berndt, K.A. Khor, and E.F. Lugscheider, Ed., ASM International, 2001, p 409-416
5. F. Gärtner, C. Borchers, T. Stoltenhoff, H. Kreye, and H. Assadi, Numerical and Microstructural Investigations of the Bonding Mechanism in Cold Spraying, *Thermal Spray 2003: Advancing the Science and Applying the Technology,* May 5-8, 2003 (Orlando, FL), C. Moreau and B. Marple, Ed., ASM International, 2003, Vol 1, p 1-8
6. D. Raybould, The Cold Welding of Powders by Dynamic Compaction, *Int. J. Powder Metall. Powder Technol.,* Vol 16 (No. 1), 1980, p 9-19
7. D. Raybould, D.G. Morris, and G.A. Cooper, A New Powder Metallurgy Method, *J. Mater. Sci.,* (No. 14), 1979, p 2523-2527
8. J. Vlcek, H. Huber, H. Voggenreiter, A. Fischer, H. Hallén, G. Pache, and E. Lugscheider, Kinetic Powder Compaction Applying the Cold Spray Process: A Study on Parameters, *Thermal Spray 2001: New Surfaces for a Millennium,* May 28-30, 2001 (Singapore), C.C. Berndt, K.A. Khor, and E.F. Lugscheider, Ed., ASM International, 2001, p 417-422
9. A.P. Alkimov, V.F. Kosarev, and A.N. Papyrin, A Method of Cold Gas-Dynamic Deposition, *Sov. Phys. Dokl.,* Vol 35 (No. 12), 1991, p 1047-1049
10. A.P. Alkimov, A.I. Gudilov, V.F. Kosarev, and N.I. Nesterovich, Specific Features of Microparticle Deformation upon Impact on a Rigid Barrier, *J. Appl. Mech. Tech. Phys.,* Vol 41 (No. 1), 2000, p 188-192
11. J. Vlcek, H. Huber, H. Voggenreiter, A. Fischer, E. Lugscheider, H. Hallén, and G. Pache, "Characteristics of Kinetic Powder Compaction with the Cold Spray Process," presented at Materials Week 2001, International Congress on Advanced Materials, Their Processes and Applications, *Deutsche Gesellschaff fur Materialkunde* (DGM) (Munich, Germany), Oct 2001
12. J.M. Walsh, R.G. Shreffler, and F.J. Willig, Limiting Conditions for Jet Formation in High Velocity Collisions, *J. Appl. Phys.,* Vol 24 (No. 3), 1953, p 349-359
13. H. Dell and G. Oberhofer, "Simulation zur Deformation eines sphärischen Pulverpartikels beim Kaltkinetischen Kompaktieren" ("Simulation of the Deformation of a Spherical Particle in the Cold Spray Process"), Report of MATFEM Engineering, Munich, Dec 2000 (in German)
14. R. Prümmer, *Explosivverdichtung pulvriger Substanzen,* Springer Verlag, 1987 (in German).
15. J.A. Zukas, *High Velocity Impact Dynamics*, John Wiley & Sons, 1990
16. J.R. Asay and M. Shahinpoor, *High Pressure Shock Compression of Solids,* Springer Verlag, 1993, p 7-113

17. R.J. Brejcha and S.W. McGee, Compaction with a 0.38 cal. Blank, *Am. Machinist,* Vol 106, 1962, p 63-65
18. J.M. Walsh and R.H. Christian, Equation of State of Metals from Shock Wave Measurements, *Phys. Rev.,* Vol 97 (No. 6), 1955, p 1544-1556
19. R.G. McQueen, S.P. Marsh, J.W. Taylor, J.N. Taylor, and W.J. Carter, The Equation of State of Solids from Shock Wave Studies, *High Velocity Impact Phenomena,* R. Kinslow, Ed., Academic Press, 1970, p 239-417
20. *Smithells Metals Reference Book*, 7th ed., E.A. Brandes and G.B. Brook, Ed., Butterworth Heinemann, Oxford, 1992
21. G. Welsch, R. Boyer, and E.W. Collings, *Materials Properties Handbook: Titanium Alloys,* 2nd ed., ASM International, 1998, p 483-636
22. Guide to Engineering Materials 2001, *Adv. Mater. Proc.,* Vol 158 (No. 6), 2000, p 29-152
23. H.H. Weigand and H.G. Dorst, Microstructural Changes in TiAl6V4 Alloy), DEW Technical Reports, Vol 1 (No. 3), 1963, p 108-113 (in German)
24. H. Kuchling, *Taschenbuch der Physik* (*Pocketbook of Physics*), Verlag Harri Deutsch, Thun/Frankfurt, 1989 (in German)
25. Appendix F: Tabulation of Shock Wave Parameters, *Shock Waves and High Strain Rate Phenomena in Metals,* MA. Meyer and L.E. Murr, Ed., Plenum Press, 1981, p 1061ff
26. H. Lippmann and O. Mahrenholtz, *Plastomechanik der Umformung metallischer Werkstoffe* (*Plastomechanics in Forming of Metallic Materials*), Springer Verlag, 1967 (in German)
27. Y.V. Prasad and S. Sasidhara, *Hot Working Guide, A Compendium of Processing Maps,* ASM International, 1997, p 1-24
28. W. Schatt and H. Worch, Ed., *Werkstoffwissenschaften* (*Material Science*), Deutscher Verlag für Grundstoffindustrie, Stuttgart, 1996 (in German)
29. H.J. Frost and MF. Ashby, *Deformation Mechanism Maps: The Plasticity and Creep of Metals and Ceramics,* Pergamon Press, Oxford, 1982
30. B. Lemcke and D. Raybould, Method of Compacting Powder, U.S. Patent 4,255,374 March 10, 1981
31. H. Kreye, F. Gärtner, and H.J. Richter, "High Velocity Oxy-Fuel Flame Spraying: State of the Art, New Developments and Alternatives," presented at Sixth Colloquium on High Velocity Oxygen Fuel Spraying (Erding, Germany), Gemeinschaft Thermisches Spritzen e.V. 2003
32. J. Vlcek, H. Huber, M. Englhart, D.P. Jonke, and F. Gammel, "Where Are the Limits of Cold Spray?: Ceramic Deposition," presented at Cold Spray New Horizons in Surfacing Technology (Albuquerque, NM), Sept 2002